REVIEW ARTICLE

Review on volumetric energy density: influence on morphology and mechanical properties of Ti6Al4V manufactured via laser powder bed fusion

Minhalina Ahmad Buhairi[1] · Farhana Mohd Foudzi[1] · Fathin Iliana Jamhari[1] · Abu Bakar Sulong[1] · Nabilah Afiqah Mohd Radzuan[1] · Norhamidi Muhamad[1] · Intan Fadhlina Mohamed[1] · Abdul Hadi Azman[1] · Wan Sharuzi Wan Harun[2] · M S H Al-Furjan[3]

Abstract

Various laser powder bed fusion (LPBF) process parameters must be considered as they can independently affect the properties of end-product. However, many studies simply examine one or two LPBF process parameters. Laser power, scan speed, scan spacing, and layer height are the four primary LPBF process parameters that contribute to volumetric energy density (VED) used in LPBF. VED is often used as an optimization metric for LPBF process parameters, because it takes all four major parameters into consideration. Thus, this paper focuses on the effect of VED on the morphology and properties of part, and also discusses on the interrelationship between all four parameters. Common range used for each parameter is 70–400 W for laser power, 70–1800 mm/s for scan speed, 50–140 μm for scan spacing, and 20–50 μm for layer height. It can be seen as the VED increased, the microstructure of as-built titanium alloy Ti6Al4V components exhibited smaller α' martensite size and larger columnar β grain. High VED can also reduce porosity and defect formation, which will help in increasing part density. The lowest surface roughness reported for LPBF Ti6Al4V is 4.91 μm. Meanwhile, the maximum microhardness obtained is 443 HV and the highest tensile strength achieved is 1400 MPa. The VED used for studies that obtained these results are in the range of 55–65 J/mm^3. Thus, it can be concluded that the most suitable VED for LPBF printing of Ti6Al4V is around 55–65 J/mm^3.

Keywords Laser powder bed fusion · Volumetric energy density · Process parameters · Morphology · Mechanical properties · Ti6Al4V

1 Introduction

One of the nine pillars introduced in the fourth industrial revolution (IR 4.0) is three-dimensional (3D) printing or additive manufacturing (AM). The metal AM field offers the possibility of fabricating a wide range of materials with complex geometry features and applications, as stated by Lewandowski and Seifi [1] and Ghani et al. [2]. Moreover, metal AM technologies help in manufacturing parts that are difficult to machine as reported by Wasono et al. [3]. According to research conducted by ARC Advisory Group [4], aerospace, automotive, and defense industries are the largest markets for metal AM in 2018. The common practice for many automotive sector manufacturers with AM is prototyping purposes because conventional methods and AM have yet to coincide in a fully automated environment. Meanwhile, in the aerospace industry, Sacco and Moon [5] reported that such industry is more focused on printing designs with intricate details while using less material that aims for reducing fuel consumption. Furthermore, since parts can be fabricated on-site using AM technologies, the self-sufficiency nature of military operations can

✉ Farhana Mohd Foudzi
farhana.foudzi@ukm.edu.my

1 Department of Mechanical and Manufacturing Engineering, Faculty of Engineering and Built Environment, Universiti Kebangsaan Malaysia, 43600 Bangi, Selangor, Malaysia

2 Faculty of Mechanical Engineering, Universiti Malaysia Pahang, 26600 Pekan, Pahang, Malaysia

3 State Key Laboratory of Mechanics and Control of Mechanical Structures, Nanjing University of Aeronautics and Astronautics, Nanjing 210016, People's Republic of China

be supported as mentioned by Vora and Sanyal [6]. Metal 3D printing is also prevalent in the medical industry as Guo et al. [7] and Duan et al. [8] reported that the technology aids in individualization (e.g., customized implants) and surgical cost reduction.

According to ISO/ASTM 52900:2015, technologies in AM can be categorized into seven categories, including four metal AM technologies which are powder bed fusion (PBF), direct energy deposition (DED), material jetting, and binder jetting. Blakey-Milner et al. [9] and Lee et al. [10] reported that among the four technologies, only PBF and DED are already at high technology readiness level (TRL). Laser powder bed fusion (LPBF) is one of the commercially available PBF process, alongside electron powder bed fusion (EPBF). LPBF is also known as selective laser melting (SLM), direct metal laser sintering (DMLS), and Laser-CUSING, which are trademarked terms by SLM Solutions Group AG, EOS GmbH, and Concept Laser, respectively. In this paper, only the term LPBF is used to avoid confusion. Among the various methods in the metal AM field, LPBF is a promising technique due to its numerous advantages. First, Pal et al. [11] reported LPBF can produce top quality parts from metal powders as it allows homogeneous build-up to almost full density. Besides, the LPBF system acknowledges a wide range of materials for fabrication such as titanium (Ti), stainless steel, aluminium (Al), cobalt-chromium (CoCr), and even gold (Au), as stated by Aboulkhair et al. [12]. The performance of these LPBF-fabricated parts is

comparable to those produced using conventional methods, which will be discussed in Sect. 5. However, due to large thermal gradient present in LPBF, it can introduce huge residual stresses and further explanation can be found in studies done by Mercelis and Kruth [13], Xiao et al. [14], Liu et al. [15] and Chao et al. [16]. The residual stresses can be countered using stress-relief treatment such as annealing or hot isostatic pressing (HIP), where the treatment can also alter the microstructure which eventually will affect the mechanical properties of the treated parts.

Figure 1 illustrates a simplified schematic of the LPBF process. The first step of LPBF process begins with the development of a 3D model using a computer-aided design (CAD) software or produced using a 3D scanner. A support structure for the model will be generated and this model will then be sliced into a stack of two-dimensional (2D) layers. The stack of 2D layers, which consists of both internal and external geometry features, will then be loaded into the LPBF machine to begin the printing process. A thin layer of metal powder will be uniformly deposited on the substrate plate using a roller before a focused laser beam melts the powder bed. After the plate is lowered down by one-layer thickness, a new layer will be applied and melted to form a successive layer that is metallurgically bonded with the previous layer. This process will be repeated until a 3D object or component is fully built. To avoid oxidation and contamination, this printing process is done with high purity shielding gas. Due to rapid repeated heating and cooling process, high

Fig. 1 Schematic of the LPBF system. This work is a derivative of [17] by Materialgeeza under CC BY-SA 3.0 license
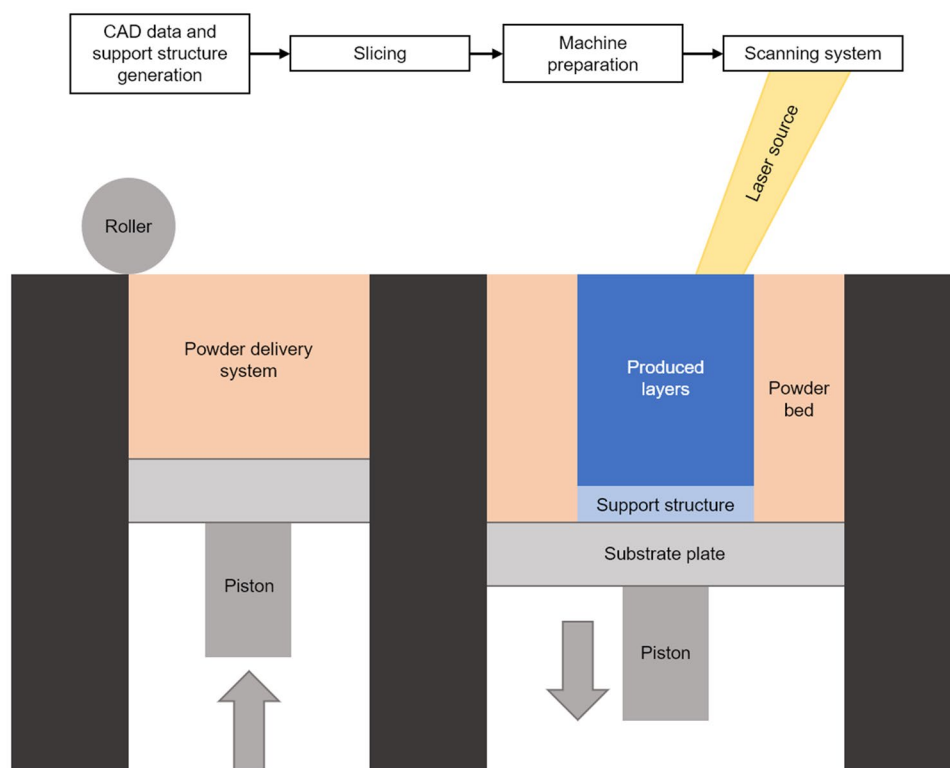
internal residual stresses are likely and can be countered by pre-heating the build plate or heat treating the end-product.

One of commonly fabricated materials using LPBF is Ti6Al4V alloy, or also known as Ti64 alloy which consists of Ti, Al, and vanadium (V). This alloy is an American Society for Testing and Materials (ASTM) Grade 5 and Grade 23 Ti. Ti Grade 23 is the higher purity version of Ti Grade 5, as it contains lower levels of oxygen (O), nitrogen (Ni), carbon (C), and iron (Fe) compared to Ti grade 5. Ti Grade 23 is also known as Ti6Al4V Extra Low Interstitials (ELI). It is noteworthy that in this paper, Ti6Al4V alloy refers to both Ti grade. Majumdar et al. [18] stated Ti6Al4V is an alpha (α)-beta (β) Ti alloy that is widely used in biomedical applications, such as prosthesis and joint replacement due to this biomaterial's low density, high strength-to-weight ratio, high corrosion resistance, excellent wear properties, and most importantly, high biocompatibility. Since Ti6Al4V is a very versatile material, this alloy is also used in the automotive, aerospace, and tooling industries, as mentioned by Liu et al. [19] and Tan et al. [20]. Nevertheless, due to its low thermal conductivity and high toughness, this material is categorized as a hard-to-machine material. Furthermore, as IR 4.0 encourages mass customization, Dilberoglu et al. [21] stated that there is a limit in manufacturing Ti6Al4V parts with the desired shape using current conventional methods; thus making LPBF the preferable method in manufacturing Ti6Al4V parts.

Presently, there is an interest in optimizing the process parameters of LPBF method to produce Ti6Al4V parts with excellent mechanical performance. As the two popular methods in metal AM field are LPBF and EPBF, a comparison in publications number over the past 10 years is made in Fig. 2. For LPBF, the keywords used to search for papers are LPBF, SLM, DMLS, and laser cusing. Selective laser sintering (SLS) is also included as sometimes researcher mistakenly used that term, although SLS is not for metal AM. Meanwhile for EPBF, the keywords used are EPBF, electron beam melting (EBM), and selective electron beam melting (SEBM). Both searches used the same keywords for Ti6Al4V which are Ti6Al4V, Ti-6Al-4V, Ti64, and TC4. Figure 2 shows that for the past 10 years, studies on LPBF are exponentially increasing compared to EPBF, demonstrating the high interest in LPBF technology. Generally, volumetric energy density (VED) is used as an optimization metric for LPBF process parameters, because it is not biased toward certain parameters. Thus, it can be observed that research focusing on the VED used during LPBF printing is also steadily increasing over the past 5 years.

Therefore, this paper aims to examine the process parameters that contribute to the VED of LPBF, compile and analyze the VED generated by the process parameters from different studies, and address the influence of VED on the morphology and mechanical performance of Ti6Al4V parts produced via LPBF. Web of Science is used to find articles and proceeding papers to be reviewed using these keywords: (TS = (laser powder bed fusion OR selective laser melting OR direct metal laser sintering OR laser cusing OR selective laser sintering)) AND (TS = (Ti6Al4V OR Ti-6Al-4V OR Ti64 OR TC4)). From each paper, the value of properties (i.e., surface roughness, microhardness, and tensile properties) with the associated VED, are evaluated. It is worth noting that this paper only focused on samples that do not use any heat treatment after LPBF process as heat treatment can change the properties of manufactured parts. Some of the key findings in this paper are summarized in Table 1. This table focused on studies that reported the highest and lowest value of surface roughness, microhardness, and tensile properties of LPBF-fabricated Ti6Al4V parts.

Fig. 2 Number of publications (articles and proceeding papers) with keywords "LPBF and Ti6Al4V", "EPBF and Ti6Al4V", and "VED and LPBF and Ti6Al4V" over the years (Web of Science, 11 March 2022)
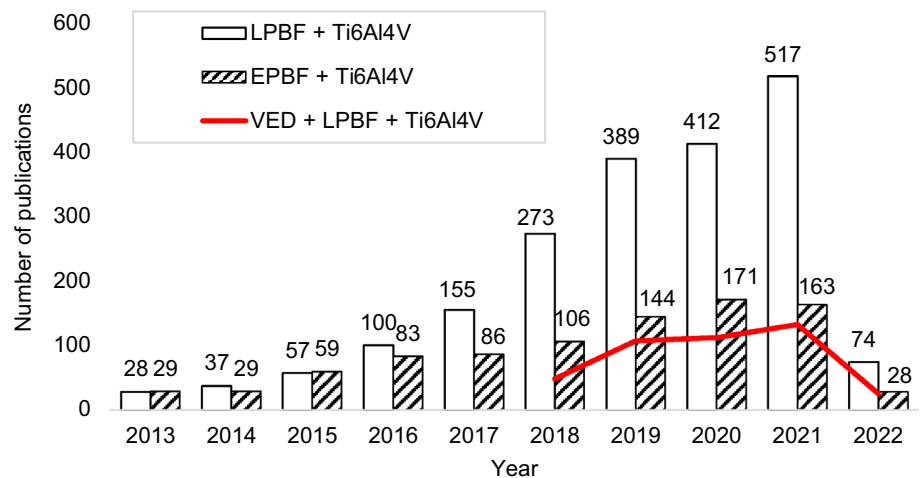
Table 1 Process parameters used during LPBF printing for Ti6Al4V parts with significant properties

Author (year)	Machine model	Process parameters					VED, E_v (J/mm^3)	Key findings
		Laser spot diameter (μm)	Laser power, P (W)	Scan speed, v (mm/s)	Scan spacing, d (μm)	Layer height, t (μm)		
Pal et al. (2019) [22]	Concept Laser mLab	110	75	600	77	25	65	Produced sample with the lowest surface roughness reported (4.91 μm) Low scan speed induced low cooling rate which caused less spattering
Zhu et al. (2016) [23]	Renishaw AM250	70	200	600	110	50	61	Reported the highest microhardness value of 443 HV Contains a fully acicular α' martensitic microstructure
Wang et al. (2019) [24]	SLM 280HL	90	200	1150	100	30	58	Reported the highest ultimate tensile strength (UTS) of Ti6Al4V manufactured via LPBF (1400 MPa) May be closely related to low porosity level produced by the parameter set
Mierzejewska et al. (2019) [25]	EOSINT M280	87	170	1300	100	30	44	Produced sample with the highest surface roughness reported (21.06 μm)
Kaya et al. (2019) [26]	Concept Laser M LabR	~50	95	1350	90	25	31	Produced sample with the lowest microhardness reported (332 HV)
Fiocchi et al. (2020) [27]	modified Renishaw AM400	70	100	1250	80	30	36	Produced sample with the lowest UTS of 938 MPa and elongation of 5.9%

2 Process parameters of LPBF

Although the LPBF process seems relatively simple, there are three vital aspects that need to be understood as it can affect the fabricated parts: material, design, and process. The materials currently used in LPBF fabrication are limited to commercially available alloys because LPBF research is mostly focused on processing alloys that suit the available manufacturing methods, as mentioned by Aboulkhair et al. [12]. Since the LPBF method uses rapid repetitive heating and cooling mechanism, it is vital to understand this mechanism before developing new alloy systems. Besides, design plays a crucial role in LPBF fabrication. Lightweight components can be produced using topology optimization; and by manipulating the design to minimize the support

structure, fabrication time and post-processing cost can be reduced.

For process-related parameters, Spears and Gold [28] have listed 50 key parameters in LPBF which can be divided into four classifications, i.e., (i) parameters of laser and scanning, (ii) properties of powder material, (iii) properties of the powder bed and parameters of recoat, and (iv) parameters of the build environment. Some laser and scanning parameters are peak power of machine, scan speed, scan spacing, and scan strategy used. Powder material involved properties such as particle morphology and particle size distribution. For powder bed, density and layer height of powder must be considered. Lastly, oxygen level and pressure are two of the build environment parameters. Some parameters can be controlled as they can be easily manipulated using the

present LPBF method. From all the parameters presented by Spears and Gold [28], only a few controlled parameters can be directly changed during the LPBF process such as laser power, scan speed, scan spacing, and layer height. Figure 3 depicts these four parameters which contribute to the VED used in LPBF. It is worth noting that the terms scanning speed, hatch spacing, and layer thickness in the figure are similar to the terms used in this paper for scan speed, scan spacing, and layer height, respectively.

2.1 Laser power

Dilip et al. [30] stated that laser power and scan speed control melting and solidification rates. Laser power is the amount of energy delivered by the laser to the powder layers. The laser power cannot be too low because enough laser power is needed to fully melt the powder layers. Pal et al. [31] asserted that although a too low laser power can induce partial melting which leads to incomplete fusion of the powder layers, very high laser power needs to be avoided as it can induce the formation of a deep keyhole, which will introduce pores as seen in Fig. 4a.

2.2 Scan speed

Spierings et al. [32] reported that scan speed plays a vital role in affecting the density and microstructure of a part, because a low scan speed can lead to irregularities and distortion. In contrast, a high scan speed can induce balling phenomenon. Balling occurs due to insufficient wetting with surrounding parts when using low VED produced by high

Fig. 3 An illustration of all four parameters that contribute to the VED used in LPBF, reused with permission from Yap et al. [29]

scan speed and low laser power. Melt pool of low VED has high surface tension and to reduce the surface tension, balling will form which can be seen in Fig. 4b. LPBF-fabricated Ti6Al4V parts that contain balling are commonly found to have interlayer bonding disrupted, porosity introduced, and surface quality degraded, as stated by Pal et al. [33].

2.3 Scan spacing

The third parameter which is scan spacing, is also known as hatch spacing, hatch distance, or track width. Scan spacing is the overlap or the gap between two neighboring laser paths. Larimian et al. [35] and Shi et al. [36] found that the amount of overlapping must be appropriately chosen to avoid improper melting of particles. A small scan spacing will result in too much overlap, which will then cause the fabrication time to be longer. Conversely, Munro [37] stated that large scan spacing can limit the maximum layer height that can be used.

2.4 Layer height

Layer height is the thickness of each powder layer on the substrate plate of the LPBF machine. Generally, the mentioned layer height does not include the first and the finishing layers as these layers do not follow the parameters of the other layers. The height of the powder layers must be at least tall enough for the parts to be manufactured. A layer thickness that is too high must be avoided as it can induce balling, dimensional inaccuracy, and incomplete melting. Partial melting will occur when there is not enough time for the laser to completely reach the whole powder layer height.

2.5 Other parameters

Other than scan spacing, laser spot diameter or also known as laser beam diameter, can also enhance productivity rate. A study done by Sow et al. [38] shows that larger spot diameter is preferable due to reduction of scan lines which decreased the fabrication time. Larger spot diameter also helps in decreasing spatters and powder bed degradation when paired with low VED during printing. In powder bed degradation, the redeposition of spatters causes a local loss of powder homogeneity.

Besides, scan strategy also helps in reducing defects such as large residual stresses and balling effect. Scan strategy is the method in which the laser beam moves during the printing process. Jia et al. [39] reported that, for a single-layer scan, the scan strategy varies according to scan directions, scan sequences, scan vector rotation angles, scan vector lengths, scan times, and scan spacing. Suitable scan directions and sequences can reduce accumulated heat and influence the temperature gradient of surrounding powder.
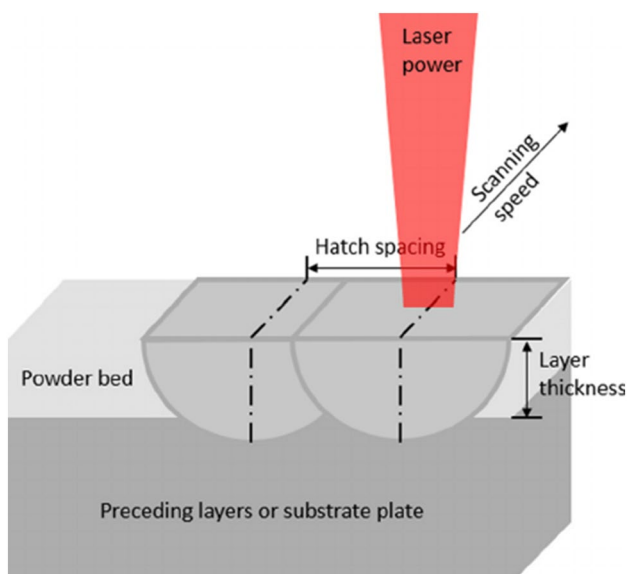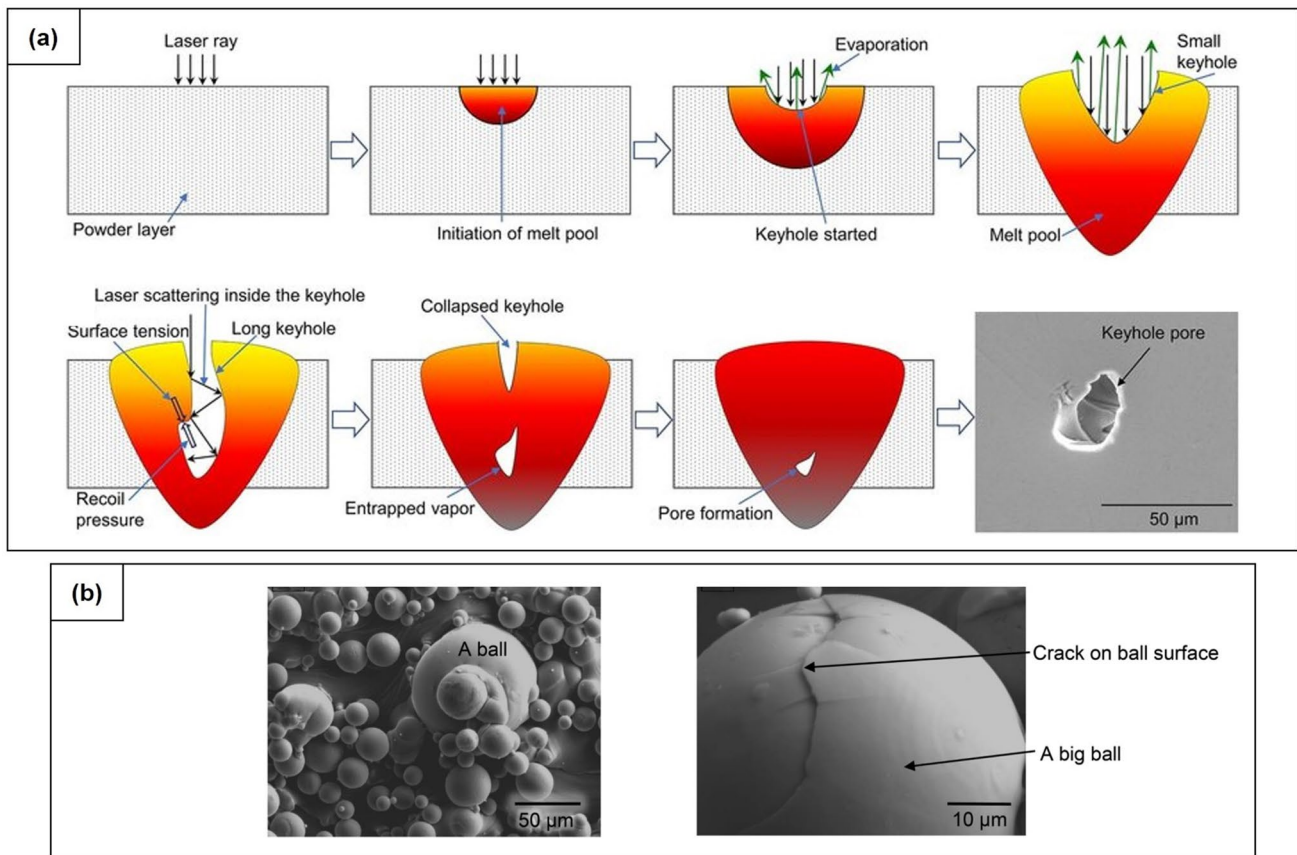
Fig. 4 **a** Keyhole formation which induce pore, reused with permission from Pal et al. [31] under CC BY-NC-ND 4.0 license and **b** balling effect shown in LPBF pure Ti, reused with permission from Attar et al. [34]

3 Volumetric energy density in LPBF

The key parameters in LPBF can also be separated into three categories, which are (i) laser parameters (e.g., laser power, scan speed, and scan spacing), (ii) powder bed parameters such as layer height, and (iii) material properties (e.g., density and specific heat capacity). All these facets are mutually interactive and choosing the most optimum parameters for an application is vital as it can affect the density and performance of the end-products as mentioned by Wang et al. [40]. A commonly used metric to optimize the process parameters of LPBF is the VED which is also known as volumetric energy concentration.

The VED, which is denoted as E_v in Eq. 3, is derived from the first two formulas as follows:

$$E_L = \frac{P}{v} \tag{1}$$

$$E_A = \frac{P}{v \times d} \tag{2}$$

$$E_V = \frac{P}{v \times d \times t} \tag{3}$$

where P stands for output laser power (W), v stands for scan speed (mm/s), d stands for scan spacing (μm), and t stands for layer height of the powder (μm). Equation 1 is the formula for linear energy density, E_L (J/mm), whereas Eq. 2 is the formula for areal energy density, E_A (J/mm^2). Meanwhile, Eq. 3 is known as the formula for VED, E_V (J/mm^3) and is the most frequently mentioned in the literature. It is noteworthy that this paper only focused on studies that used VED. The VED used in fabricating Ti6Al4V parts for different LPBF machine are shown in Fig. 5. It should be noted that LSNF-1 is a self-built system. In general, VED is used in the range of 30 to 210 J/mm^3. Some self-built systems often use a very high VED, while commercial LPBF systems tend to use VED around 60 J/mm^3. This is because self-built systems like LSNF-1 can produce very high output power which can be seen in studies by Meng et al. [41] and Yang et al. [42], and this induces a higher possible VED that can be used. As scan speed can be calculated using point

Fig. 5 The VED used by different printer brand in fabricating Ti6Al4V parts [22–27, 36, 40, 42–114]
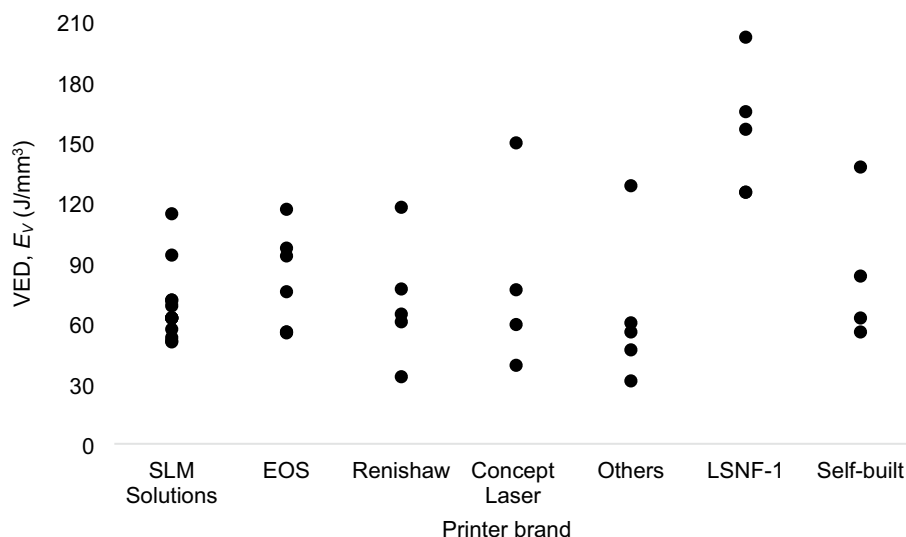
distance (µm) and exposure time (µs), Eq. 3 can be further derived to form another VED equation as follows:

$$E_V = \frac{P}{\frac{P_d}{e_t} \times d \times t} \tag{4}$$

where P_d is the point distance (µm) and e_t is the exposure time of the laser (µs).

Most studies used laser power in the range of 70–400 W, while there are studies that used laser power of almost 1000 W. Besides, the scan speed used to produce the LPBF-fabricated parts varied greatly from around 70–1800 mm/s. Scan spacing used in most LPBF studies usually ranging around 50–140 µm. Meanwhile, for layer height, the powder thickness used differed slightly from 20 to 50 µm, as it is typically anticipated that better product properties will result from using a thinner powder layer as mentioned by Tan et al. [20]. However, build time will take significantly longer as a trade-off. Sufficient VED (up to a certain boundary, usually ranging between 50 and 150 J/mm³) can result in satisfactory material properties, where at higher VED, a larger amount of melting will occur which leads to printed parts with high density. Therefore, these four process parameters need to be accurately adjusted to fabricate parts with the highest possible density. It is important to note that each parameter can independently affect the LPBF process, and different parameter combinations, while having the same VED, can induce different thermal behaviors. These thermal behaviors will lead to variation of microstructure and mechanical performance, as reported by Prashanth et al. [115] who observed a difference of 14% in the UTS of two samples that used the same VED but with different laser power. However, VED can still be used as a guideline in choosing the most optimum process parameters. This is because Ti6Al4V parts that are manufactured using VED ranging around 60 J/mm³

seem to have excellent physical and mechanical performance compared to the other VED, as seen in Table 1.

4 Morphology of LPBF Ti6Al4V

4.1 Microstructure

At room temperature, Ti6Al4V contains dual (α + β) phase in which Al helps in stabilizing α phase while V helps in stabilizing β phase. Due to extreme heating, melting, and cooling rates of LPBF, various phases of Ti6Al4V can be produced using this method (e.g., α, α' martensite, and β). The dual phase will transform to β phase during melting before turning into liquid phase. The liquid phase will then convert to the former β phase during cooling, and depending on the cooling rate, the β phase will transform back to the dual phase or becoming α' phase. Zhang and Attar [116] reported that the LPBF-fabricated parts usually have a finer microstructure compared to those fabricated using conventional methods because of LPBF's extreme cooling rate. Xu et al. [50] also added that finer β grains can be produced by reducing the layer height of the powder.

Figure 6 shows the microstructure of as-built LPBF Ti6Al4V parts, which consists of β grain and four types of α' martensite. Yang et al. [118] concluded that depending on their size, martensite can be classified as primary, secondary, tertiary, and quaternary. Biggest α' martensite is deemed as the primary α' martensite, while the finest one is called quaternary α' martensite. Majumdar et al. [119] added that high laser power causes multiple heating and cooling cycles of the powder layer, which will produce dendrites perpendicular to the applied layer. Although α' martensite helps to increase the corrosion resistance nature of Ti6Al4V,

Fig. 6 Microstructure of as-built LPBF Ti6Al4V which consists of: **a** a former β-grain with boundary and α′ martensite, and **b** and **c** four types of α′ martensite, reused with permission from Drstvenšek et al. [117] under CC BY-NC-ND 4.0 license
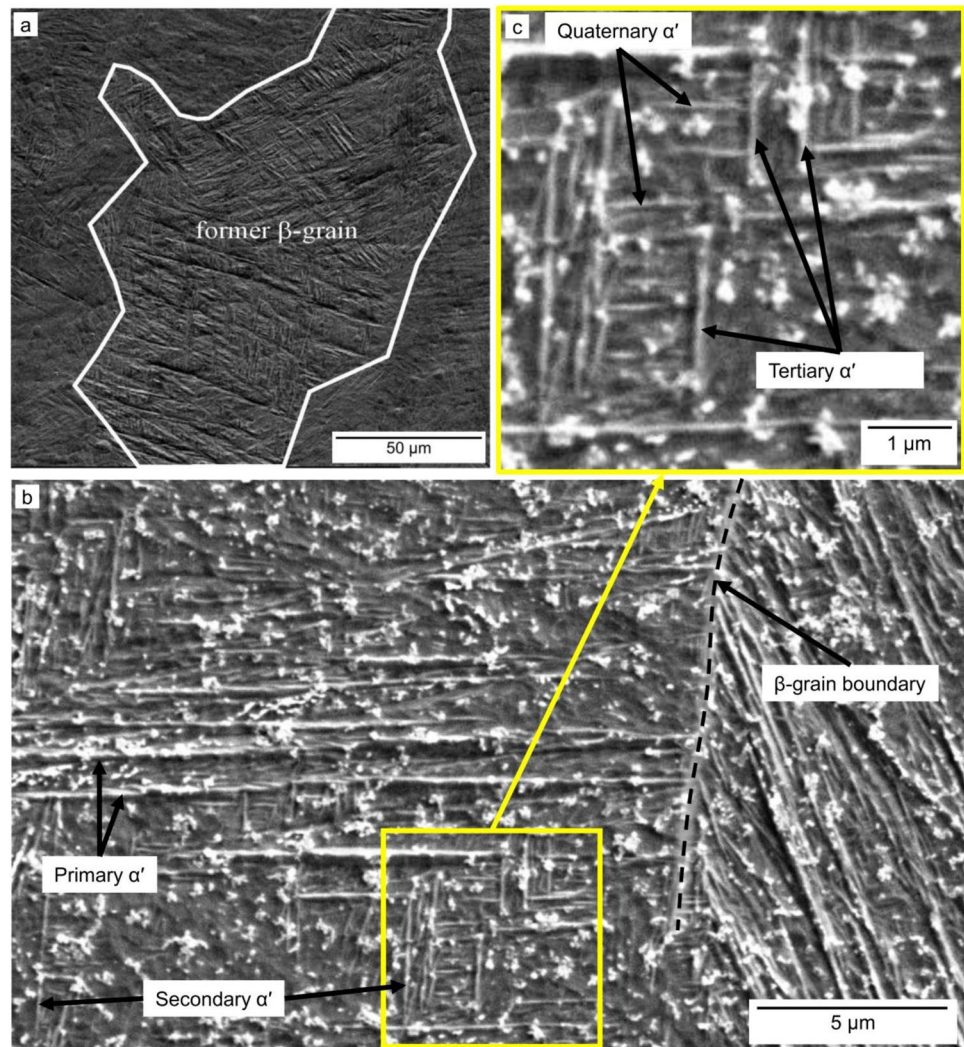
columnar β grain structures are needed as they can increase the part's tensile strength.

Microstructure of Ti6Al4V can also be changed depending on the VED used during LPBF printing as shown in Fig. 7. It can be seen that microstructures of parts using VED of 38–51 J/mm^3 consists of predominantly acicular α' martensite. This is due to the extremely rapid cooling rate of LPBF and as the VED increased, the cooling rate also increased causing the martensite size to become smaller, as mentioned by Do and Li [65]. Xu et al. [50] found that with proper LPBF temperature, (ultrafine α-lamellar + β particle) microstructure can be seen in parts that used VED of 61 J/mm^3. This may be due to the lower cooling rate and thermal gradient of the VED compared to a higher value of VED. As the VED increased to 202 J/mm^3, relatively finer α' martensite can be seen in the Ti6Al4V microstructure.

Han et al. [47] reported that high VED produced smaller α' martensite size and bigger columnar β grain. In their work, it was found that as the VED increased from 75 to 250 J/mm^3, the width of α' martensite decreased from 51 to 47 μm. The spacing of α' martensite also decreased, while the width of columnar β grain increased from 42 to 52 μm. High VED induces higher temperature gradient and higher cooling rate. This temperature gradient reduces the potential of nucleation due to a decreased undercooling; thus, producing a coarse columnar β grain structure, making the average width of grain bigger. Besides, the cooling rate helps in refining the α' martensite by inducing a faster nucleation rate as mentioned by Han et al. [47]. This is also supported by Xu et al. [50] who found that the width of α/α′ martensite become smaller as the VED increased.

4.2 Pores' morphology

The LPBF-fabricated parts' density depends on the chemical composition and the resulting porosity from the process. The density can be measured using the Archimedes, pycnometer, or optical methods. In theory, LPBF can fabricate a fully
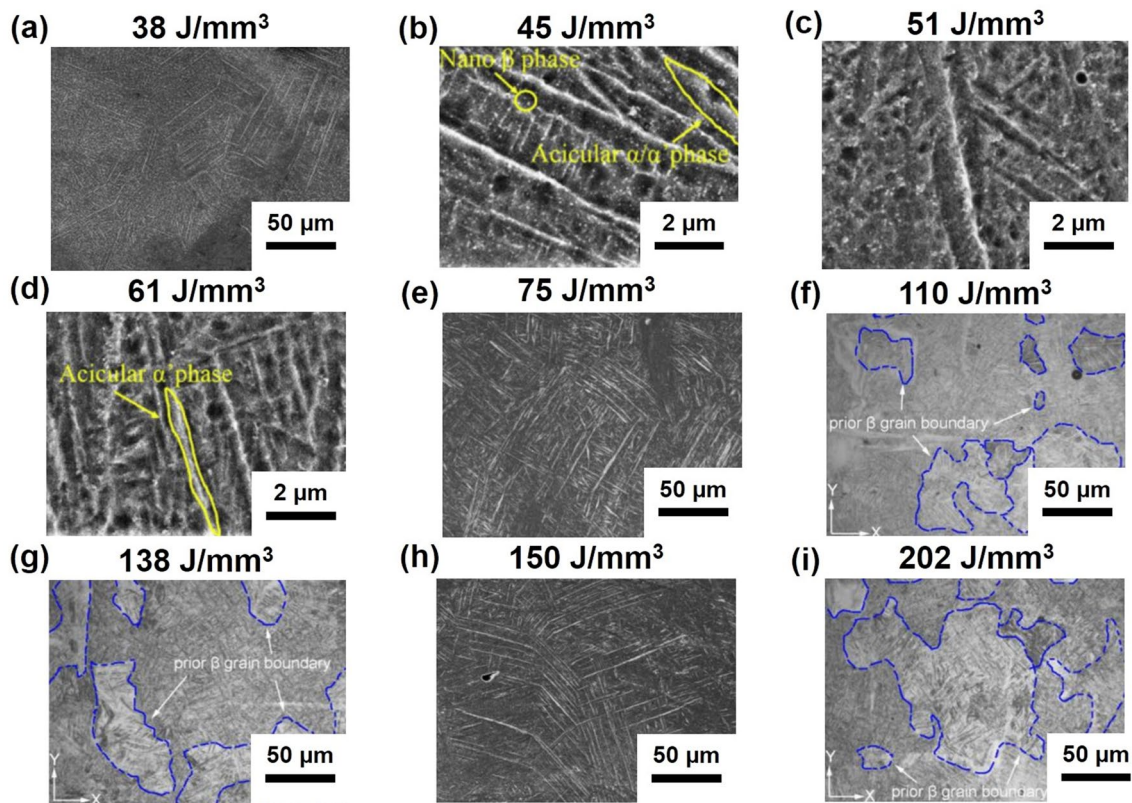
Fig. 7 Microstructures of as-built Ti6Al4V manufactured using different VED of LPBF, reused with permission from: **a**, **e**, and **h** Do and Li [65], **b–d** Xu et al. [50] and **f**, **g**, and **i** Han et al. [47]

dense part as mentioned by Wang et al. [40]. However, due to insubstantial process parameters, pores will always be present. The only difference is whether the porosity level is manageable because an uncontrolled porosity level can initiate microcracks and adiabatic shear bands, which can lead to poor performance of fabricated parts as stated by Liu and Shin [120]. Industrial application, especially for a load-bearing structural part, requires a high part density (which will contribute to high mechanical performance) induced by the low porosity level. Meanwhile, Hudák et al. [121], Mehboob et al. [122], and Mohammadi et al. [123] stated that applications such as Ti6Al4V implants need a controlled

porous structure to reduce the "stress-shielding" effect. Stress shielding happens when bone density is decreased as a result of an implant removing stress from the bone.

Pores are formed in LPBF-fabricated parts due to the liquid–solid phase transformation during the solidification process. Two types of pores can be present in LPBF parts, i.e., gas pores and lack-of-fusion pores, as shown in Fig. 8. Gas pores are characterized by their spherical or elliptical shapes, while lack-of-fusion pores are often larger and have irregular shapes with some sharp tips. On one hand, gas pores are present when gas bubbles could not escape the molten pool in time due to the rapid solidification

Fig. 8 Types of pore present in LPBF-fabricated parts: **a** gas pore and **b** lack-of-fusion pore, reused with permission from Liu et al. [125]
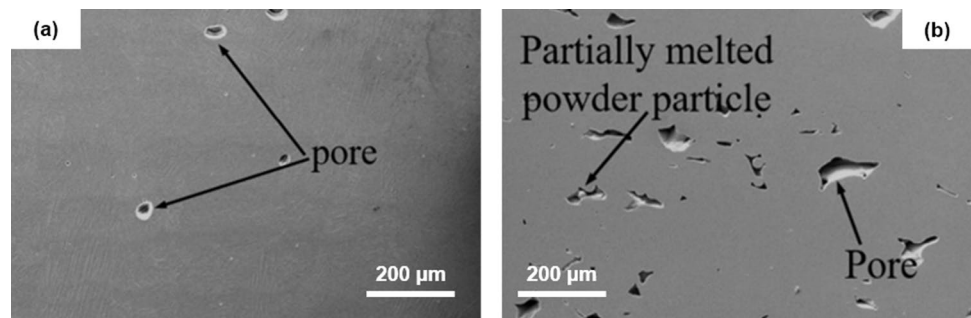
induced by the high VED, causing them to be trapped in the solidified parts as mentioned by Zhou et al. [124]. On the other hand, Liu et al. [125] found that lack-of-fusion pores form due to insufficient VED (e.g., too low laser power or too high scan speed) to melt a disproportionate amount of powders. Consequently, inadequate melting and incomplete interlayer bonding may occur.

Lack-of-fusion pores are more dangerous than gas pores, because they can greatly influence the mechanical properties of the fabricated parts since these pores are usually distributed at the boundary zone of two adjacent layers, which are typically aligned in the building direction as reported by Liu et al. [125]. Liu and Shin [120] mentioned that when the parts are under a uniaxial tensile load parallel to the building direction, the sharp tips of the lack-of-fusion pores will accumulate stresses and act as a crack initiator, leading to premature failure. These pores can be reduced by increasing the VED used to melt the powder layers. Meanwhile, Narra et al. [126] stated gas pores can be avoided by using dense metal powders or gas-atomized powders, instead of sponge powders, as the feedstock. Gas pores can also be reduced by decreasing the powder's layer height so that the gas at the bottom of the molten pool can escape in time. Although porosity can be managed by optimizing the process parameters, the lowest

it can be reduced is 0.012% with the help of HIP process as seen in a study done by Kasperovich and Hausmann [127].

Based on Eq. 3, VED is the product of relationship of the four parameters (i.e., laser power, scan speed, scan spacing, and layer height), which will indirectly help in controlling the porosity which leads to a higher densification of parts. In short, VED can be used as an indicator to produce high-density parts. Figure 9a–c shows the microstructural difference found by Bartolomeu et al. [63] between samples that used the VED of 46, 79, and 93 J/mm^3, respectively. Higher densification level can be seen in Fig. 9c compared to Fig. 9a, b. The sample in Fig. 9c also contained a lower number of process defects. Higher densification level attained by the sample in Fig. 9c led to higher hardness and shear strength. Meanwhile, in Fig. 9d, e, samples were produced using the same VED (42 J/mm^3) but with different laser power and scan spacing. These two samples showed that the final characteristics of Ti6Al4V parts can also be influenced by each parameter. This is because the microstructures and porosity levels in the two samples are not the same, despite using the same VED, as found by Bartolomeu et al. [63].

The relationship between VED and relative density is shown in Fig. 10, in which it can be seen that relative density of parts increased with increasing VED before decreasing after VED reached 60 J/mm^3 (study done by Junfeng and Zhengying [128]) and 138 J/mm^3 (study done by Han et al.
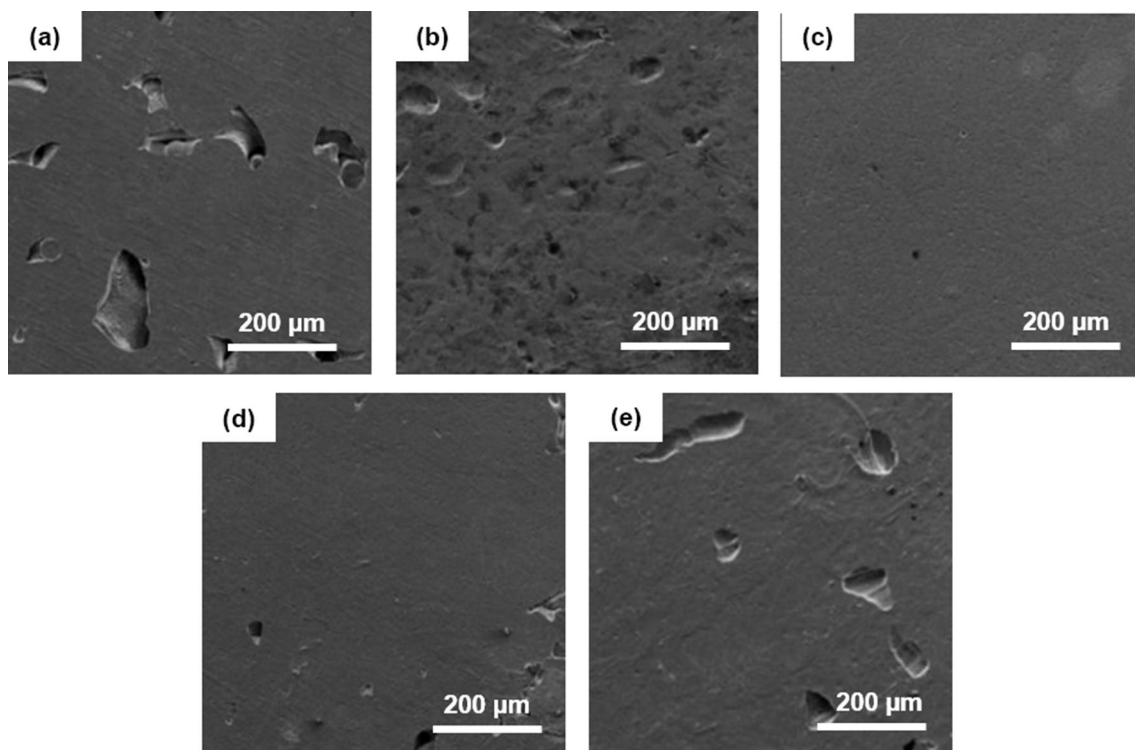
Fig. 9 Microstructures of Ti6Al4V manufactured using LPBF with the VED of **a** 46 J/mm^3, **b** 79 J/mm^3, **c** 93 J/mm^3, and **d** and **e** 42 J/mm.^{3}, reused with permission from Bartolomeu et al. [63]
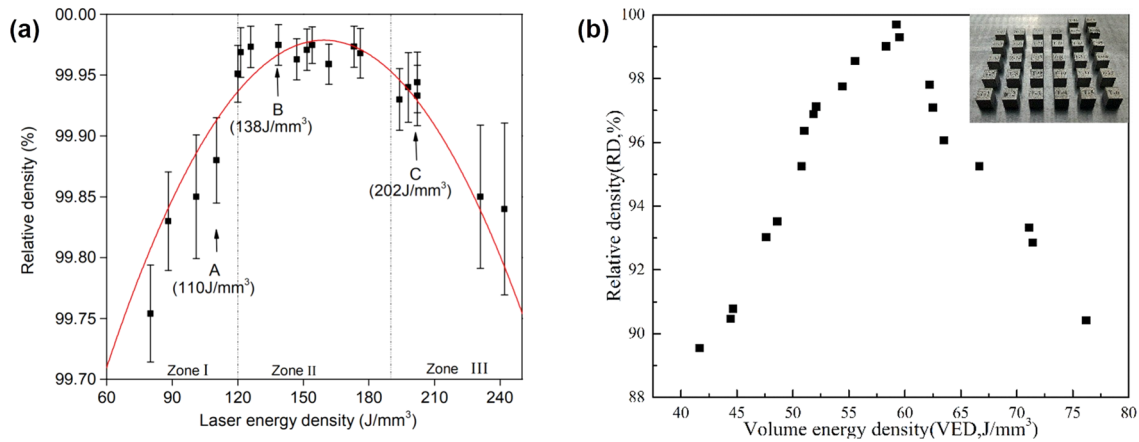
Fig. 10 Variation of relative density of Ti6Al4V parts produced using different VED of LPBF, reused with permission from **a** Han et al. [47] and **b** Junfeng and Zhengying [128] under CC BY 3.0 license

[47]). It is noted that the term VED is designated as laser energy density in Fig. 10a. On one hand, Junfeng and Zhengying [128] attributed this occurrence is due to low value of VED which produced weak bonding between the powder layers and un-melted powder particles, making the relative density become low. On the other hand, when the VED is too high, it will increase the depth of melting tracks and may cause element evaporation which will decrease the part density. Han et al. [47] also supported that weak metallurgical bonding formed using low VED will reduce the relative density of parts and too high VED can cause evaporation of powders. However, these two studies reported different values of VED that managed to produce near-dense Ti6Al4V parts. This may be due to different process parameter sets used by both studies, in which Junfeng and Zhengying [128] used higher laser power and scan speed compared to Han et al. [47]. Although laser beam diameter is not included in the VED equation, different laser beam diameters used for both studies might also be the reason, because beam diameter can result in different intensities and thus varying the weld pool dimensions. Besides, the methods used to measure density in both studies are also different, in which Han et al. [47] used optical method and Junfeng and Zhengying [128] used Archimedes method.

5 Characteristics of LPBF Ti6Al4V

This section covers the properties of Ti6Al4V parts manufactured using LPBF printing. The presented values in this section are extracted from the reported values by the referred papers used for this review. As mentioned before, the value of properties from each paper with the associated VED, will be compiled graphically. There are ten different studies for each VED group (i.e., less than 61 J/mm^3, 61 to 70 J/mm^3,

71 to 80 J/mm^3, 81 to 90 J/mm^3, and more than 90 J/mm^3). The graphs in this section (i.e., Figs. 11, 12, 13) are meant as reference for expected values of properties at different range of VED.

5.1 Surface roughness

Figure 11 illustrates the summary of reported work on surface roughness of Ti6Al4V parts fabricated using different VED in LPBF. Most studies of surface roughness reviewed in this paper were conducted on the top section of parts. It can be seen that the surface roughness of Ti6Al4V parts decreased as the VED increased to around 80 J/mm^3, before it increased when the VED is more than 80 J/mm^3. The highest surface roughness reported is 21.06 μm by Mierzejewska et al. [25], which is due to the high porosity level induced by low VED. Since low surface roughness of fabricated parts is preferred especially in the medical industry (less than two
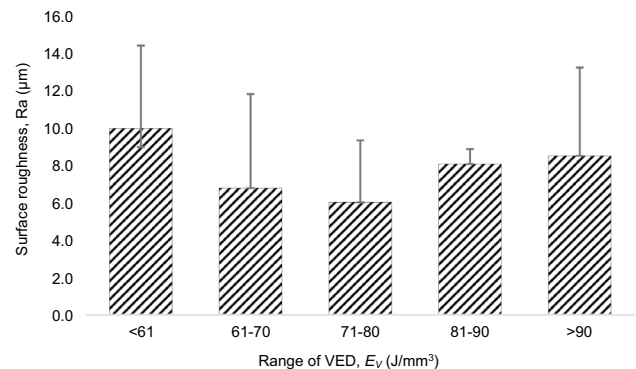
Fig. 11 Reported study on surface roughness of Ti6Al4V parts fabricated using different VED of LPBF [22–25, 46, 48, 51, 53, 57–61, 65, 66, 72, 80, 82, 87, 89, 93, 94, 98, 102, 105, 109–111, 113, 114]
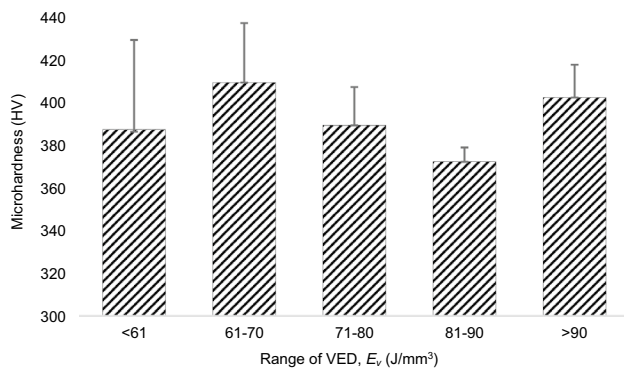
Fig. 12 Reported value of microhardness of Ti6Al4V parts obtained using different VED of LPBF [23–26, 42–45, 47–49, 51, 62, 63, 65, 66, 69, 71–74, 78, 79, 84, 86–90, 93–95, 99, 101, 102, 104–106, 112, 133]

μm), it can be deduced that VED used during LPBF printing must be around 61 to 80 J/mm^3. This is supported by Do and Li [65] who reported that surface quality of samples increased by increasing the VED from 37.5 to 75 J/mm^3. However, the quality decreased when the energy is increased to 150 J/mm^3. This is because too high VED widens the scan track due to heat conduction and induces balling which decrease the surface quality.

At high temperature (above the vaporization temperature), metal vapor is created and caused powder to blow out from the printing zone. Such phenomenon leads to higher surface roughness. Pal et al. [129] asserted that the recoil pressure helps in decreasing the surface tension of the pool and thus reducing the surface roughness. Scan speed also has a vital role in determining the surface roughness of produced parts. A high scan speed will result in a higher cooling rate and a reduction in fabrication time which can be seen in a study done by Dilip et al. [30]. Nonetheless, a scan speed

that is too high must be avoided as it can induce higher shear stress which will then lead to ball formation. Tian et al. [130] and Chen et al. [131] have deduced that a low hatch spacing would be better to achieve higher densification of parts, but the distance must not be too small as it can result in a considerable overlap which will increase the surface roughness. This is because a significant overlap promotes the attachment of particles onto the surface.

5.2 Microhardness

Microhardness is a relatively easy and quick way to determine the mechanical performance of produced parts due to its small sample size requirement. Some of the Ti6Al4V parts' microhardness reported in the literature are shown in Fig. 12. It can be seen that microhardness of Ti6Al4V samples increased as the VED increased to 70 J/mm^3 before promptly decreased. The microhardness increased again when VED reaches more than 90 J/mm^3. The average microhardness of the LPBF-fabricated Ti6Al4V parts reported is around 400 to 450 HV, which is higher than the microhardness of parts produced via conventional method as seen in a comparison study done by Attar et al. [132]. The lowest microhardness achieved is 332 HV by Kaya et al. [26], while the highest microhardness is reported by Zhu et al. [23] with a value of 443 HV.

Since VED influences the microstructure and pore formation of Ti6Al4V parts fabricated by LPBF, microhardness of Ti6Al4V is also affected. This is because Sui et al. [84] stated that parts with high density have higher resistance to plastic deformation, which leads to higher microhardness. Besides, Han et al. [47] asserted that the decrease in width and spacing of α' martensite due to high VED helps in improving the microhardness value. This is because finer grain in Ti6Al4V causes hardening of material. Meanwhile,

Fig. 13 Variation on tensile properties of Ti6Al4V parts printed using different VED of LPBF [22–25, 27, 36, 40, 42–44, 47–50, 52, 53, 64, 67–73, 75, 76, 79–81, 83, 85, 86, 88, 89, 91, 92, 94–97, 100, 103, 107, 135]
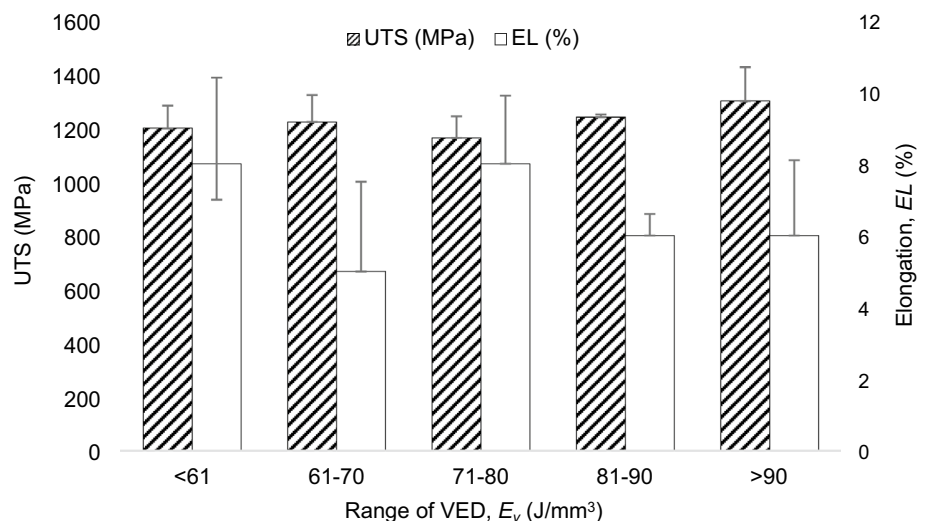
Liu and Shin [120] observed that irregular defects such as lack-of-fusion pores, can cause lower microhardness due to more freedom for plastic deformation, compared to gas pores. In a nutshell, higher VED used during LPBF printing for Ti6Al4V can encourage grain refinement which helps in improving the microhardness value.

5.3 Tensile properties

Literature data of tensile properties of Ti6Al4V parts fabricated using LPBF are shown in Fig. 13. It is worth noting that the range of values reported is quite broad because of difference in process parameters used, machine used, and powder used. This leads to the lack of trend between VED used and the tensile properties obtained. The maximum UTS and elongation reported are 1400 MPa by Wang et al. [24] and 11.7% by Lu et al. [79], respectively. To achieve this maximum UTS, VED of 114 J/mm^3 was used. This finding concurs with the tensile properties illustrated in Fig. 13, in which VED that is more than 90 J/mm^3 produced parts with the highest tensile strength. As the ASTM casting standard for tensile strength and elongation [134] is 860 MPa and 8%, respectively, it can be concluded that tensile properties achieved for Ti6Al4V parts produced by LPBF are comparable to those manufactured using conventional methods.

Tensile properties of Ti6Al4V parts can be affected by the VED used as VED affects part density. This is because tensile strength is directly affected by part density. Corner point in non-spherical pores can initiate microcracks which will reduce the tensile strength of specimens as reported by Liu et al. [125]. As mentioned before, high VED produces high temperature gradient, and this will induce spattering phenomenon which can be seen in study done by Ur Rehman et al. [136]. This phenomenon can generate lack of material and consequently decrease the overall mass in the action zone. This will lead to higher brittleness and thus, producing parts with low tensile strength.

The very fine microstructure of Ti6Al4V fabricated using LPBF also helps in improving the tensile strength, compared to parts that are made using conventional methods. Xu et al. [50] stated smaller width of α' martensite will produce smaller α colony size of martensitic microstructure and a decrease in slip length. The smaller colony size will hinder the dislocation movement and limit plastic deformation; thus, tensile strength will be increased. Besides, tensile strength also depends on the orientation of columnar β grain. Tao et al. [135] reported that if the tensile testing was done width-wise, the possibility of crack to initiate and propagate along the β grains are high, because β grains are parallel to the building direction making the tensile stress perpendicular to the grain boundaries.

6 Conclusion and future works

Among all the AM technologies, LPBF is one of the promising methods and it has been extensively studied by researchers over the past few years. Since past research conducted has managed to fabricate high-density end-products, the focus of LPBF studies has changed the direction toward the optimization of select process parameters. A common optimization metrics used is the VED of LPBF. This is because it consists of four dominant process parameters which are laser power, scan speed, scan spacing, and layer height. VED is utilized to successively melt layers of metal powder, which will then lead to the fabrication of parts with diverse microstructure and mechanical properties as shown in Sects. 4 and 5. Table 2 concludes VED ranges that are the most optimum to obtain Ti6Al4V parts with excellent properties.

Nevertheless, the VED is not the sole factor that will determine the properties of the LPBF-fabricated parts. This is because the formula used to calculate VED only include four process parameters while dismissing critical factors such as laser spot diameter and scan strategy. Besides, two different parameter sets can contribute to a similar amount of VED, while producing parts that have different mechanical performance. Therefore, some future research directions that can be considered are:

1. The interdependencies of all four parameters (i.e., laser power, scan speed, scan spacing, and layer height). This can be done to investigate the reliability of VED

Table 2 Optimum range for VED on properties of LPBF-fabricated Ti6Al4V parts

Properties	Optimum range of VED, E_V (J/mm^3)	Remarks
Relative density	More than 60	Depends on process parameters combinations used
Surface roughness	61–80	Surface roughness increased when the energy is increased more than 80 J/mm^3 This is because too high VED widens the scan track and induces balling
Microhardness	61–70	Decrease in width and spacing of α' martensite due to high VED helps in improving the microhardness
Tensile strength	More than 90	High VED induces smaller α' martensite width which will produce smaller α colony Smaller colony size will hinder the dislocation movement and limit plastic deformation; thus, tensile strength will be increased

as an optimization metric for LPBF; because different parameter combinations can induce different thermal behaviors which will then vary the microstructure and performance of the end-products.

2. The standardization of powder properties. This must be conducted before a patterned LPBF processing window for Ti6Al4V parts can be produced. Currently, the powder used in studies depends on the machine model used since most LPBF manufacturers provide their own powders. This leads to inconsistency in the performance of the fabricated part due to different powder properties. As such, the optimized process parameters obtained might not be applicable for different LPBF machine models.

3. The evolution of microstructure before and after post-processing. Although the presence of α' martensite in the as-built part aids in the corrosion resistance of Ti6Al4V, columnar β grain structures are required to improve the part's tensile strength. Thus, post-processing is usually done to transform the martensitic phase in order to counter defects, even though theoretically, LPBF can alter the microstructure during printing process to obtain the desired part properties.

Author contributions MAB writing—original draft, data curation, investigation, formal analysis. FMF writing—original idea, methodology, supervision, formal analysis, writing—review and editing, validation. FIJ conceptualization, investigation, data curation. ABS writing—review and editing, validation, supervision. NAMR conceptualization, writing—review and editing, supervision. NM conceptualization, formal analysis, validation. IFM investigation, methodology, formal analysis. AHA formal analysis, data curation, investigation. WSWH conceptualization, investigation, formal analysis, validation. MSHA-F validation, writing-review and editing.

Availability of data and materials The authors declare that the data supporting the findings of this study are available within the article.

Code availability Not applicable.

Declarations

Conflict of interest The authors have no conflicts of interest to declare that are relevant to the content of this article.

References

1. Lewandowski JJ, Seifi M (2016) Metal additive manufacturing: a review of mechanical properties. Annu Rev Mater Res 46:151–186. https://doi.org/10.1146/annurev-matsci-070115-032024

2. Ghani SAC, Zakaria MH, Harun WSW, Zaulkafilai Z (2017) Dimensional accuracy of internal cooling channel made by selective laser melting (SLM) and direct metal laser sintering (DMLS) processes in fabrication of internally cooled cutting tools. MATEC Web Conf 90:01058. https://doi.org/10.1051/matecconf/20179001058

3. Wasono RS, Wahab DA, Azman AH (2019) Additive manufacturing for repair and restoration in remanufacturing: An overview from object design and systems perspectives. Processes 7(11):802. https://doi.org/10.3390/pr7110802

4. Wanke F (2019) Additive manufacturing in automotive and aerospace and defense industries disruptive. ARC Advisory Group. https://bit.ly/2WDjq5a. Accessed 30 Aug 2021

5. Sacco E, Moon SK (2019) Additive manufacturing for space: space and promises. Int J Adv Manuf Technol 105(10):4123–4146. https://doi.org/10.1007/s00170-019-03786-z

6. Vora HD, Sanyal S (2020) A comprehensive review: metrology in additive manufacturing and 3D printing technology. Prog Addit Manuf 5(4):319–353. https://doi.org/10.1007/s40964-020-00142-6

7. Guo Y, Ren L, Xie K, Wang L, Yu B, Jiang W, Zhao Y, Hao Y (2020) Functionalized TiCu/Ti–Cu–N-coated 3D-printed porous Ti6Al4V scaffold promotes bone regeneration through BMSC recruitment. Adv Mater Interfaces 7(6):1901632. https://doi.org/10.1002/admi.201901632

8. Duan Y, Liu X, Zhang S, Wang L, Ding F, Song S, Chen X, Deng B, Song Y (2020) Selective laser melted titanium implants play a positive role in early osseointegration in type 2 diabetes mellitus rats. Dent Mater J 39(2):214–221. https://doi.org/10.4012/dmj.2018-419

9. Blakey-Milner B, Gradl P, Snedden G, Brooks M, Pitot J, Lopez E, Leary M, Berto F, du Plessis A (2021) Metal additive manufacturing in aerospace: a review. Mater Des 209:110008. https://doi.org/10.1016/j.matdes.2021.110008

10. Lee JY, Nagalingam AP, Yeo SH (2021) A review on the state-of-the-art of surface finishing processes and related ISO/ASTM standards for metal additive manufactured components. Virtual Phys Prototyp 16(1):68–96. https://doi.org/10.1080/17452759.2020.1830346

11. Pal S, Lojen G, Kokol V, Drstvenšek I (2019) Reducing porosity at the starting layers above supporting bars of the parts made by selective laser melting. Powder Technol 355:268–277. https://doi.org/10.1016/j.powtec.2019.07.059

12. Aboulkhair NT, Simonelli M, Parry L, Ashcroft I, Tuck C, Hague R (2019) 3D printing of aluminium alloys: additive manufacturing of aluminium alloys using selective laser melting. Prog Mater Sci 106:100578. https://doi.org/10.1016/j.pmatsci.2019.100578

13. Mercelis P, Kruth JP (2006) Residual stresses in selective laser sintering and selective laser melting. Rapid Prototyp 12(5):254–265. https://doi.org/10.1108/13552540610707013

14. Xiao Z, Chen C, Zhu H, Hu Z, Nagarajan B, Guo L, Zeng X (2020) Study of residual stress in selective laser melting of Ti6Al4V. Mater Des 193:108846. https://doi.org/10.1016/j.matdes.2020.108846

15. Liu Y, Yang Y, Wang D (2016) A study on the residual stress during selective laser melting (SLM) of metallic powder. Int J Adv Manuf Technol 87(1):647–656. https://doi.org/10.1007/s00170-016-8466-y

16. Chao Q, Thomas S, Birbilis N, Cizek P, Hodgson PD, Fabijanic D (2021) The effect of post-processing heat treatment on the microstructure, residual stress and mechanical properties of selective laser melted 316L stainless steel. Mater Sci Eng A 821:141611. https://doi.org/10.1016/j.msea.2021.141611

17. Materialgeeza (2019) SLS system schematic. Wikimedia Commons. https://commons.wikimedia.org/wiki/File:Selective_laser_melting_system_schematic.jpg. Accessed 31 Aug 2021

18. Majumdar T, Eisenstein N, Frith JE, Cox SC, Birbilis N (2018) Additive manufacturing of titanium alloys for orthopedic applications: a materials science viewpoint. Adv Eng Mater 20(9):1800172. https://doi.org/10.1002/adem.201800172

19. Liu Y, Liang C, Liu W, Ma Y, Liu C, Zhang C (2018) Dilution of Al and V through laser powder deposition enables a continuously compositionally Ti/Ti6Al4V graded structure. J Alloys Compd 763:376–383. https://doi.org/10.1016/j.jallcom.2018.05.289

20. Tan JH, Wong WLE, Dalgarno KW (2017) An overview of powder granulometry on feedstock and part performance in the selective laser melting process. Addit Manuf 18:228–255. https://doi.org/10.1016/j.addma.2017.10.011

21. Dilberoglu UM, Gharehpapagh B, Yaman U, Dolen M (2017) The role of additive manufacturing in the era of industry 4.0. Procedia Manuf 11:545–554. https://doi.org/10.1016/j.promfg.2017.07.148

22. Pal S, Gubeljak N, Hudak R, Lojen G, Rajtukova V, Predan J, Kokol V, Drstvensek I (2019) Tensile properties of selective laser melting products affected by building orientation and energy density. Mater Sci Eng A 743:637–647. https://doi.org/10.1016/j.msea.2018.11.130

23. Zhu Y, Chen X, Zou J, Yang H (2016) Sliding wear of selective laser melting processed Ti6Al4V under boundary lubrication conditions. Wear 368:485–495. https://doi.org/10.1016/j.wear.2016.09.020

24. Wang Z, Xiao Z, Tse Y, Huang C, Zhang W (2019) Optimization of processing parameters and establishment of a relationship between microstructure and mechanical properties of SLM titanium alloy. Opt Laser Technol 112:159–167. https://doi.org/10.1016/j.optlastec.2018.11.014

25. Mierzejewska ZA, Hudák R, Sidun J (2019) Mechanical properties and microstructure of DMLS Ti6Al4V alloy dedicated to biomedical applications. Mater 12(1):176. https://doi.org/10.3390/ma12010176

26. Kaya G, Yildiz F, Hacisalihoğlu A (2019) Characterization of the structural and tribological properties of medical Ti6Al4V alloy produced in different production parameters using selective laser melting. 3D Print Addit Manuf 6(5):253–261. https://doi.org/10.1089/3dp.2019.0017

27. Fiocchi J, Biffi CA, Scaccabarozzi D, Saggin B, Tuissi A (2020) Enhancement of the damping behavior of Ti6Al4V alloy through the use of trabecular structure produced by selective laser melting. Adv Eng Mater 22(2):1900722. https://doi.org/10.1002/adem.201900722

28. Spears TG, Gold SA (2016) In-process sensing in selective laser melting (SLM) additive manufacturing. Integr Mater Manuf Innov 5(1):16–40. https://doi.org/10.1186/s40192-016-0045-4

29. Yap CY, Chua CK, Dong ZL, Liu ZH, Zhang DQ, Loh LE, Sing SL (2015) Review of selective laser melting: materials and applications. Appl Phys Rev 2(4):041101. https://doi.org/10.1063/1.4935926

30. Dilip JJS, Zhang S, Teng C, Zeng K, Robinson C, Pal D, Stucker B (2017) Influence of processing parameters on the evolution of melt pool, porosity, and microstructures in Ti-6Al-4V alloy parts fabricated by selective laser melting. Prog Addit Manuf 2(3):157–167. https://doi.org/10.1007/s40964-017-0030-2

31. Pal S, Gubeljak N, Hudák R, Lojen G, Rajťúková V, Brajlih T, Drstvenšek I (2020) Evolution of the metallurgical properties of Ti-6Al-4V, produced with different laser processing parameters, at constant energy density in selective laser melting. Results Phys 17:103186. https://doi.org/10.1016/j.rinp.2020.103186

32. Spierings AB, Dawson K, Uggowitzer PJ, Wegener K (2018) Influence of SLM scan-speed on microstructure, precipitation of Al₃Sc particles and mechanical properties in Sc- and Zr-modified Al–Mg alloys. Mater Des 140:134–143. https://doi.org/10.1016/j.matdes.2017.11.053

33. Pal S, Lojen G, Hudak R, Rajtukova V, Brajlih T, Kokol V, Drstvenšek I (2020) As-fabricated surface morphologies of Ti-6Al-4V samples fabricated by different laser processing parameters in selective laser melting. Addit Manuf 33:101147. https://doi.org/10.1016/j.addma.2020.101147

34. Attar H, Calin M, Zhang LC, Scudino S, Eckert J (2014) Manufacture by selective laser melting and mechanical behavior of commercially pure titanium. Mater Sci Eng A 593:170–177. https://doi.org/10.1016/j.msea.2013.11.038

35. Larimian T, Kannan M, Grzesiak D, AlMangour B, Borkar T (2020) Effect of energy density and scanning strategy on densification, microstructure and mechanical properties of 316L stainless steel processed via selective laser melting. Mater Sci Eng A 770:138455. https://doi.org/10.1016/j.msea.2019.138455

36. Shi X, Ma S, Liu C, Chen C, Wu Q, Chen X, Lu J (2016) Performance of high layer thickness in selective laser melting of Ti6Al4V. Mater 9(12):975. https://doi.org/10.3390/ma9120975

37. Munro C (2017) Effect of hatch spacing on bead geometry during blown powder laser additive manufacturing. Canadian Defence Information Database. https://cradpdf.drdc-rddc.gc.ca/PDFS/unc277/p805479_A1b.pdf. Accessed 31 Aug 2021

38. Sow MC, De Terris T, Castelnau O, Hamouche Z, Coste F, Fabbro R, Peyre P (2020) Influence of beam diameter on Laser Powder Bed Fusion (L-PBF) process. Addit Manuf 36:101532. https://doi.org/10.1016/j.addma.2020.101532

39. Jia H, Sun H, Wang H, Wu Y, Wang H (2021) Scanning strategy in selective laser melting (SLM): a review. Int J Adv Manuf Technol 113(9):2413–2435. https://doi.org/10.1007/s00170-021-06810-3

40. Wang YM, Kamath C, Voisin T, Li Z (2018) A processing diagram for high-density Ti-6Al-4V by selective laser melting. Rapid Prototyp J 24(9):1469–1478. https://doi.org/10.1108/RPJ-11-2017-0228

41. Meng L, Zhao J, Lan X, Yang H, Wang Z (2020) Multi-objective optimisation of bio-inspired lightweight sandwich structures based on selective laser melting. Virtual Phys Prototyp 15(1):106–119. https://doi.org/10.1080/17452759.2019.1692673

42. Yang J, Han J, Yu H, Yin J, Gao M, Wang Z, Zeng X (2016) Role of molten pool mode on formability, microstructure and mechanical properties of selective laser melted Ti-6Al-4V alloy. Mater Des 110:558–570. https://doi.org/10.1016/j.matdes.2016.08.036

43. Liu J, Sun Q, Wang X, Li H, Guo K, Sun J (2019) Achieving Ti6Al4V alloys with both high strength and ductility via selective laser melting. Mater Sci Eng A 766:138319. https://doi.org/10.1016/j.msea.2019.138319

44. Hattal A, Chauveau T, Djemai J, Fouchet JJ, Bacroix B, Dirras G (2019) Effect of nano-yttria stabilized zirconia addition on the microstructure and mechanical properties of Ti6Al4V parts manufactured by selective laser melting. Mater Design 180:107909. https://doi.org/10.1016/j.matdes.2019.107909

45. Xiao Z, Chen C, Hu Z, Zhu H, Zeng X (2020) Effect of rescanning cycles on the characteristics of selective laser melting of Ti6Al4V. Opt Laser Technol 12:105890. https://doi.org/10.1016/j.optlastec.2019.105890

46. Foudzi FM, Buhairi MA, Jamhari FI, Sulong AB, Radzuan NAM, Muhamad N, Harun WSW, Al-Furjan MSH (2021) Effect of energy density on properties of additive manufactured Ti6Al4V via SLM. IN: International Conference on Powder Metallurgy and Particulate Materials (Powdermet2021), pp 434–448

47. Han J, Yang J, Yu H, Yin J, Gao M, Wang Z, Zeng X (2017) Microstructure and mechanical property of selective laser melted Ti6Al4V dependence on laser energy density. Rapid Prototyp J 23(2):217–226. https://doi.org/10.1108/RPJ-12-2015-0193

48. Wang D, Dou W, Yang Y (2018) Research on selective laser melting of Ti6Al4V: Surface morphologies, optimized processing zone, and ductility improvement mechanism. Metals 8(7):471. https://doi.org/10.3390/met8070471

49. Li F, Wang Z, Zeng X (2017) Microstructures and mechanical properties of Ti6Al4V alloy fabricated by multi-laser beam selective laser melting. Mater Lett 199:79–83. https://doi.org/10.1016/j.matlet.2017.04.050

50. Xu Y, Zhang D, Guo Y, Hu S, Wu X, Jiang Y (2020) Microstructural tailoring of As-selective laser melted Ti6Al4V alloy for high mechanical properties. J Alloys Comp 816:152536. https://doi.org/10.1016/j.jallcom.2019.152536

51. Wang Z, Liu Z, Gao C, Wong K, Ye S, Xiao Z (2020) Modified wear behavior of selective laser melted Ti6Al4V alloy by direct current assisted ultrasonic surface rolling. Surf Coat Technol 381:125122. https://doi.org/10.1016/j.surfcoat.2019.125122

52. Rautio T, Hamada A, Mäkikangas J, Jaskari M, Järvenpää A (2020) Laser welding of selective laser melted Ti6Al4V: microstructure and mechanical properties. Mater Today Proc 28:907–911. https://doi.org/10.1016/j.matpr.2019.12.322

53. Nalli F, Bottini L, Boschetto A, Cortese L, Veniali F (2020) Effect of industrial heat treatment and barrel finishing on the mechanical performance of Ti6AL4V processed by selective laser melting. Appl Sci 10(7):2280. https://doi.org/10.3390/app10072280

54. Fousová M, Vojtěch D, Kubásek J, Jablonská E, Fojt J (2017) Promising characteristics of gradient porosity Ti-6Al-4V alloy prepared by SLM process. J Mech Behav Biomed Mater 69:368–376. https://doi.org/10.1016/j.jmbbm.2017.01.043

55. Fousová M, Vojtěch D, Doubrava K, Daniel M, Lin CF (2017) Influence of inherent surface and internal defects on mechanical properties of additively manufactured Ti6Al4V alloy: comparison between selective laser melting and electron beam melting. Mater 11(4):537. https://doi.org/10.3390/ma11040537

56. Borrego LP, de Jesus J, Ferreira JAM, Costa JDM, Capela C (2019) Assessment of the fatigue performance of heat-treated addictive manufactured TiAl6V4 specimens. Procedia Struct Integr 18:651–656. https://doi.org/10.1016/j.prostr.2019.08.212

57. Bartolomeu F, Dourado N, Pereira F, Alves N, Miranda G, Silva FS (2020) Additive manufactured porous biomaterials targeting orthopedic implants: a suitable combination of mechanical, physical and topological properties. Mater Sci Eng C 107:110342. https://doi.org/10.1016/j.msec.2019.110342

58. Costa MM, Lima R, Melo-Fonsesca F, Bartolomeu F, Alves N, Miranda A, Gasik M, Silva FS, Silva NA, Miranda G (2019) Driving cellular response by modulating physical and chemical properties. Mater Sci Eng C 98:705–716. https://doi.org/10.1016/j.msec.2019.01.01

59. Bartolomeu F, Abreu CS, Moura CG, Costa MM, Alves N, Silva FS, Miranda G (2019) Ti6Al4V-PEEK multi-material structures–design, fabrication and tribological characterization focused on orthopedic implants. Tribol Int 131:672–678. https://doi.org/10.1016/j.triboint.2018.11.017

60. Melo-Fonsesca F, Lima R, Costa MM, Bartolomeu F, Alves N, Miranda A, Gasik M, Silva FS, Silva NA, Miranda G (2018) The influence of the design on some of the physical and chemical interactions that drive cellular response. Mater Des 160:95–105. https://doi.org/10.1016/j.matdes.2018.08.056

61. Bartolomeu F, Sampaio M, Carvalho O, Pinto E, Alves N, Gomes JR, Silva FS, Miranda G (2017) Tribological behavior of Ti6Al4V cellular structures produced by selective laser melting. J Mech Behav Biomed Mater 69:128–134. https://doi.org/10.1016/j.jmbbm.2017.01.004

62. Bartolomeu F, Buciumeanu M, Pinto E, Alves N, Silva FS, Carvalho O, Miranda G (2017) Wear behavior of Ti6Al4V biomedical alloys processed by selective laser melting, hot pressing and conventional casting. Trans Nonferrous Met Soc China 27(4):829–838. https://doi.org/10.1016/S1003-6326(17)60060-8

63. Bartolomeu F, Faria S, Carvalho O, Pinto E, Alves N, Silva FS, Miranda G (2016) Predictive models for physical and mechanical properties of Ti6Al4V produced by selective laser melting. Mater Sci Eng A 663:181–192. https://doi.org/10.1016/j.msea.2016.03.113

64. Lui EW, Xu W, Pateras A, Qian M, Brandt M (2017) New development in selective laser melting of Ti-6Al-4V: a wider processing window for the achievement of fully lamellar α + β microstructures. JOM 69(12):2679–2683. https://doi.org/10.1007/s11837-017-2599-9

65. Do DK, Li P (2016) The effect of laser energy input on the microstructure, physical and mechanical properties of Ti-6Al-4V alloys by selective laser melting. Virtual Phys Prototyp 11(1):41–47. https://doi.org/10.1080/17452759.2016.1142215

66. Weißmann V, Drescher P, Bader R, Seitz H, Hansmann H, Laufer N (2017) Comparison of single Ti6Al4V struts made using selective laser melting and electron beam melting subject to part orientation. Metals 7(3):91. https://doi.org/10.3390/met7030091

67. Konečná R, Kunz L, Bača A, Nicoletto G (2017) Resistance of direct metal laser sintered Ti6Al4V alloy against growth of fatigue cracks. Eng Fract Mech 185:82–91. https://doi.org/10.1016/j.engfracmech.2017.03.033

68. Liang Z, Sun Z, Zhang W, Wu S, Chang H (2019) The effect of heat treatment on microstructure evolution and tensile properties of selective laser melted Ti6Al4V alloy. J Alloys Compd 782:1041–1048. https://doi.org/10.1016/j.jallcom.2018.12.051

69. Yan X, Yin S, Chen C, Huang C, Bolot R, Lupoi R, Kuang M, Ma W, Coddet C, Liao H, Liu M (2018) Effect of heat treatment on the phase transformation and mechanical properties of Ti6Al4V fabricated by selective laser melting. J Alloys Compd 764:1056–1071. https://doi.org/10.1016/j.jallcom.2018.06.076

70. He B, Wu W, Zhang L, Lu L, Yang Q, Long Q, Chang K (2018) Microstructural characteristic and mechanical property of Ti6Al4V alloy fabricated by selective laser melting. Vacuum 150:79–83. https://doi.org/10.1016/j.vacuum.2018.01.026

71. Ali H, Ghadbeigi H, Mumtaz K (2018) Effect of scanning strategies on residual stress and mechanical properties of selective laser melted Ti6Al4V. Mater Sci Eng A 712:175–187. https://doi.org/10.1016/j.msea.2017.11.103

72. Ali H, Ghadbeigi H, Mumtaz K (2018) Processing parameter effects on residual stress and mechanical properties of selective laser melted Ti6Al4V. J Mater Eng Perform 27(8):4059–4068. https://doi.org/10.1007/s11665-018-3477-5

73. Wei WH, Shen J (2018) Effect of laser energy density on microstructures and mechanical properties of selective laser melted Ti-6Al-4V alloy. Int J Mater Research 109(5):437–442. https://doi.org/10.3139/146.111615

74. Mahmoud D, Elbestawi MA, Yu B (2019) Process-structure-property relationships in selective laser melting of porosity graded gyroids. J Med Devices 13(3):031005. https://doi.org/10.1115/1.4043736

75. Xiong YZ, Gao RN, Zhang H, Dong LL, Li J, Li X (2020) Rationally designed functionally graded porous Ti6Al4V scaffolds with high strength and toughness built via selective laser melting for load-bearing orthopedic applications. J Mech Behav Biomed Mater 104:103673. https://doi.org/10.1016/j.jmbbm.2020.103673

76. Yang Y, Chen J, Wang HL, Zhang ZQ, Lu YJ, Wu SQ, Lin JX (2017) Crystallographic features of α variants and β phase for Ti-6Al-4V alloy fabricated by selective laser melting. Mater Sci Eng A 707:548–558. https://doi.org/10.1016/j.msea.2017.09.06

77. Chang K, Liang E, Huang W, Zhang X, Chen Y, Dong J, Zhang R (2020) Microstructural feature and mechanical property in different building directions of additive manufactured Ti6Al4V alloy. Mater Lett 267:127516. https://doi.org/10.1016/j.matlet.2020.127516

78. Valente EH, Jellesen MS, Somers MAJ, Christiansen TL (2020) Gaseous surface hardening of Ti-6Al-4V fabricated by selective laser melting. Surf Coatings Technol 383:125278. https://doi.org/10.1016/j.surfcoat.2019.125278

79. Lu J, Lu H, Xu X, Yao J, Cai J, Luo K (2020) High-performance integrated additive manufacturing with laser shock peening–induced microstructural evolution and improvement in mechanical properties of Ti6Al4V alloy components. Int J Mach Tools Manuf 148:103475. https://doi.org/10.1016/j.ijmachtools.2019.103475

80. Sarker A, Tran N, Rifai A, Elambasseril J, Brandt M, Williams R, Leary M, Fox K (2018) Angle defines attachment: switching the biological response to titanium interfaces by modifying the inclination angle during selective laser melting. Mater Des 154:326–339. https://doi.org/10.1016/j.matdes.2018.05.043

81. Xu W, Brandt M, Sun S, Elambasseril J, Liu Q, Latham K, Xia K, Qian M (2015) Additive manufacturing of strong and ductile Ti–6Al–4V by selective laser melting via in situ martensite decomposition. Acta Mater 85:74–84. https://doi.org/10.1016/j.actamat.2014.11.028

82. Foudzi FM, Buhairi MA, Jamhari FI (2020) Influence of processing parameters of selective laser melting (SLM) on additive manufactured titanium alloy (Ti6Al4V). In: Proceedings of Mechanical Engineering Research Day, pp 55–57

83. Sallica-Leva E, Caram R, Jardini AL, Fogagnolo JB (2016) Ductility improvement due to martensite α' decomposition in porous Ti-6Al-4V parts produced by selective laser melting for orthopedic implants. J Mech Behav Biomed Mater 54:149–158. https://doi.org/10.1016/j.jmbbm.2015.09.020

84. Sui Q, Li P, Wang K, Yin X, Liu L, Zhang Y, Zhang Q, Wang S, Wang L (2019) Effect of build orientation on the corrosion behavior and mechanical properties of selective laser melted Ti-6Al-4V. Metals 9(9):976. https://doi.org/10.3390/met9090976

85. Mierzejewska ZA (2019) Effect of laser energy density, internal porosity and heat treatment on mechanical behavior of biomedical Ti6Al4V alloy obtained with DMLS technology. Mater 12(14):2331. https://doi.org/10.3390/ma12142331

86. Sangregorio M, Wang N, Xie K, Zhang Z, Wang X (2018) Rapid fabrication of ion optics by selective laser melting. Rapid Prototyp J 25(2):299–307. https://doi.org/10.1108/RPJ-05-2017-0085

87. Valente EH, Gundlach C, Christiansen TL, Somers MA (2019) Effect of scanning strategy during selective laser melting on surface topography, porosity, and microstructure of additively manufactured Ti-6Al-4V. Appl Sci 9(24):5554. https://doi.org/10.3390/app9245554

88. Yan Q, Chen B, Kang N, Lin X, Lv S, Kondoh K, Li S, Li JS (2020) Comparison study on microstructure and mechanical properties of Ti-6Al-4V alloys fabricated by powder-based selective-laser-melting and sintering methods. Mater Charact 164:110358. https://doi.org/10.1016/j.matchar.2020.110358

89. Srinivasan D, Singh A, Reddy AS, Chatterjee K (2020) Microstructural study and mechanical characterisation of heat-treated direct metal laser sintered Ti6Al4V for biomedical applications. Mater Technol 37(4):260–271. https://doi.org/10.1080/10667857.2020.1830566

90. Simonelli M, Aboulkhair NT, Cohen P, Murray JW, Clare AT, Tuck C, Hague RJ (2018) A comparison of Ti-6Al-4V in-situ alloying in selective laser melting using simply-mixed and satellited powder blend feedstocks. Mater Charact 143:118–126. https://doi.org/10.1016/j.matchar.2018.05.039

91. Gong H, Dilip JJS, Yang L, Teng C, Stucker B (2017) Influence of small particles inclusion on selective laser melting of Ti-6Al-4V powder. IOP Conf Ser Mater Sci Eng 272(1):012024. https://doi.org/10.1088/1757-899X/272/1/012024

92. Ter Haar GM, Becker TH (2018) Selective laser melting produced Ti-6Al-4V: Post-process heat treatments to achieve superior tensile properties. Mater 11(1):146. https://doi.org/10.3390/ma11010146

93. Promoppatum P, Onler R, Yao SC (2017) Numerical and experimental investigations of micro and macro characteristics of direct metal laser sintered Ti-6Al-4V products. J Mater Process Technol 240:262–273. https://doi.org/10.1016/j.jmatprotec.2016.10.005

94. Suresh S, Sun CN, Tekumalla S, Rosa V, Nai SML, Wong RCW (2021) Mechanical properties and in vitro cytocompatibility of dense and porous Ti–6Al–4V ELI manufactured by selective laser melting technology for biomedical applications. J Mech Behav Biomed Mater 123:104712. https://doi.org/10.1016/j.jmbbm.2021.104712

95. Fotovvati B, Etesami SA, Asadi E (2019) Process-property-geometry correlations for additively-manufactured Ti–6Al–4V sheets. Mater Sci Eng A 760:431–447. https://doi.org/10.1016/j.msea.2019.06.020

96. Hasib MT, Ostergaard HE, Li X, Kruzic JJ (2021) Fatigue crack growth behavior of laser powder bed fusion additive manufactured Ti-6Al-4V: roles of post heat treatment and build orientation. Int J Fatigue 142:105955. https://doi.org/10.1016/j.ijfatigue.2020.105955

97. Xu Y, Lu Y, Sundberg KL, Liang J, Sisson RD (2017) Effect of annealing treatments on the microstructure, mechanical properties and corrosion behavior of direct metal laser sintered Ti-6Al-4V. J Mater Eng Perform 26(6):2572–2582. https://doi.org/10.1007/s11665-017-2710-y

98. Zhao DP, Tang JC, Nie HM, Zhang Y, Chen YK, Zhang X, Li HX, Yan M (2018) Macro-micron-nano-featured surface topography of Ti-6Al-4V alloy for biomedical applications. Rare Met 37(12):1055–1063. https://doi.org/10.1007/s12598-018-1150-7

99. Le Coz G, Piquard R, D'Acunto A, Bouscaud D, Fischer M, Laheurte P (2020) Precision turning analysis of Ti-6Al-4V skin produced by selective laser melting using a design of experiment approach. Int J Adv Manuf Technol 110(5–6):1615–1625. https://doi.org/10.1007/s00170-020-05807-8

100. Xing LL, Zhang WJ, Zhao CC, Gao WQ, Shen ZJ, Liu W (2021) Influence of powder bed temperature on the microstructure and mechanical properties of ti-6al-4v alloys fabricated via laser powder bed fusion. Mater. https://doi.org/10.3390/ma14092278

101. Liu X, Wu M, Lu P, Ye X, Miao X (2020) Corrosion behavior of GO-reinforced TC4 nanocomposites manufactured by selective

laser melting. Mater Corros 71(4):628–636. https://doi.org/10.1002/maco.201911250

102. Zhang Q, Duan B, Zhang Z, Wang J, Si C (2021) Effect of ultrasonic shot peening on microstructure evolution and corrosion resistance of selective laser melted Ti-6Al-4V alloy. J Mater Res Technol 11:1090–1099. https://doi.org/10.1016/j.jmrt.2021.01.091

103. Zhang Q, Xie J, London T, Griffiths D, Bhamji I, Oancea V (2019) Estimates of the mechanical properties of laser powder bed fusion Ti-6Al-4V parts using finite element models. Mater Des. https://doi.org/10.1016/j.matdes.2019.107678

104. Ju J, Zhao C, Kang M, Li J, He L, Wang C, Li J, Fu H, Wang J (2021) Effect of heat treatment on microstructure and tribological behavior of Ti–6Al–4V alloys fabricated by selective laser melting. Tribol Int 159:106996. https://doi.org/10.1016/j.triboint.2021.106996

105. Yeo I, Bae S, Amanov A, Jeong S (2021) Effect of laser shock peening on properties of heat-treated Ti–6Al–4V manufactured by laser powder bed fusion. Int J Precis Eng Manuf Green Technol 8(4):1137–1150. https://doi.org/10.1007/s40684-020-00234-2

106. Varela J, Arrieta E, Paliwal M, Marucci M, Sandoval JH, Gonzalez JA, McWilliams B, Murr LE, Wicker RB, Medina F (2021) Investigation of microstructure and mechanical properties for Ti-6Al-4V alloy parts produced using non-spherical precursor powder by laser powder bed fusion. Mater 14(11):3028. https://doi.org/10.3390/ma14113028

107. Yang L, Zhicong P, Ming L, Yonggang W, Di W, Changhui S, Shuxin L (2019) Investigation into the dynamic mechanical properties of selective laser melted Ti-6Al-4V alloy at high strain rate tensile loading. Mater Sci Eng A 745:440–449. https://doi.org/10.1016/j.msea.2019.01.010

108. Chiu TM, Mahmoudi M, Dai W, Elwany A, Liang H, Castaneda H (2018) Corrosion assessment of Ti-6Al-4V fabricated using laser powder-bed fusion additive manufacturing. Electrochim Acta 279:143–151. https://doi.org/10.1016/j.electacta.2018.04.189

109. Milton S, Morandeau A, Chalon F, Leroy R (2016) Influence of Finish machining on the surface integrity of Ti6Al4V produced by selective laser melting. Procedia CIRP 45:127–130. https://doi.org/10.1016/j.procir.2016.02.340

110. Li Z, Kucukkoc I, Zhang DZ, Liu F (2018) Optimising the process parameters of selective laser melting for the fabrication of Ti6Al4V alloy. Rapid Prototyp J 24(1):150–159. https://doi.org/10.1108/RPJ-03-2016-0045

111. Elsayed M, Ghazy M, Youssef Y, Essa K (2018) Optimization of SLM process parameters for Ti6Al4V medical implants. Rapid Prototyp J 25(3):433–447. https://doi.org/10.1108/RPJ-05-2018-0112

112. Qiao B, Dong C, Tong S, Kong D, Ni X, Zhang H, Wang L, Li X (2019) Anisotropy in α′ martensite and compression behavior of Ti6Al4V prepared by selective laser melting. Mater Res Express 6(12):126548. https://doi.org/10.1088/2053-1591/ab5741

113. Sato Y, Tsukamoto M, Masuno S, Yamashita Y, Yamashita K, Tanigawa D, Abe N (2016) Investigation of the microstructure and surface morphology of a Ti6Al4V plate fabricated by vacuum selective laser melting. Appl Phys A Mater Sci Process 122(4):4–8. https://doi.org/10.1007/s00339-016-9996-8

114. Yu H, Yang J, Yin J, Wang Z, Zeng X (2017) Comparison on mechanical anisotropies of selective laser melted Ti-6Al-4V alloy and 304 stainless steels. Mater Sci Eng A 695:92–100. https://doi.org/10.1016/j.msea.2017.04.031

115. Prashanth KG, Scudino S, Maity T, Das J, Eckert J (2017) Is the energy density a reliable parameter for materials synthesis by selective laser melting. Mater Res Lett 5(6):386–390. https://doi.org/10.1080/21663831.2017.1299808

116. Zhang LC, Attar H (2016) Selective laser melting of titanium alloys and titanium matrix composites for biomedical applications: a review. Adv Eng Mater 18(4):463–475. https://doi.org/10.1002/adem.201500419

117. Drstvenšek I, Zupanič F, Bončina T, Brajlih T, Pal S (2021) Influence of local heat flow variations on geometrical deflections, microstructure, and tensile properties of Ti-6Al-4 V products in powder bed fusion systems. J Manuf Process 65:382–396. https://doi.org/10.1016/j.jmapro.2021.03.054

118. Yang J, Yu H, Yin J, Gao M, Wang Z, Zeng X (2016) Formation and control of martensite in Ti-6Al-4V alloy produced by selective laser melting. Mater Des 108:308–318. https://doi.org/10.1016/j.matdes.2016.06.117

119. Majumdar T, Bazin T, Massahud Carvalho Ribeiro E, Frith JE, Birbilis N (2019) Understanding the effects of PBF process parameter interplay on Ti-6Al-4V surface properties. PLoS ONE 14(8):e0221198. https://doi.org/10.1371/journal.pone.0221198

120. Liu S, Shin YC (2019) Additive manufacturing of Ti6Al4V alloy: a review. Mater Des 164:107552. https://doi.org/10.1016/j.matdes.2018.107552

121. Hudák R, Schnitzer M, Králová ZO, Gorejová R, Mitrík L, Rajťúková V, Tóth T, Kovačević M, Riznič M, Oriňaková R, Živčák J (2021) Additive manufacturing of porous Ti6Al4V alloy: geometry analysis and mechanical properties testing. Appl Sci 11(6):2611. https://doi.org/10.3390/app11062611

122. Mehboob H, Tarlochan F, Mehboob A, Chang SH, Ramesh S, Harun WS, Kadirgama K (2020) A novel design, analysis and 3D printing of Ti-6Al-4V alloy bio-inspired porous femoral stem. J Mater Sci Mater Med 31(9):1–4. https://doi.org/10.1007/s10856-020-06420-7

123. Mohammadi H, Sepantafar M, Muhamad N, Sulong AB (2021) How does scaffold porosity conduct bone tissue regeneration. Adv Eng Mater 23(10):2100463. https://doi.org/10.1002/adem.202100463

124. Zhou B, Zhou J, Li H, Lin F (2018) A study of the microstructures and mechanical properties of Ti6Al4V fabricated by SLM under vacuum. Mater Sci Eng A 724:1–10. https://doi.org/10.1016/j.msea.2018.03.021

125. Liu W, Chen C, Shuai S, Zhao R, Liu L, Wang X, Hu T, Xuan W, Li C, Yu J, Wang J, Ren Z (2020) Study of pore defect and mechanical properties in selective laser melted Ti6Al4V alloy based on X-ray computed tomography. Mater Sci Eng A 797:139981. https://doi.org/10.1016/j.msea.2020.139981

126. Narra SP, Wu Z, Patel R, Capone J, Paliwal M, Beuth J, Rollett A (2020) Use of non-spherical hydride-dehydride (HDH) powder in powder bed fusion additive manufacturing. Addit Manuf 34:101188. https://doi.org/10.1016/j.addma.2020.101188

127. Kasperovich G, Hausmann J (2015) Improvement of fatigue resistance and ductility of TiAl6V4 processed by selective laser melting. J Mater Process Technol 220:202–214. https://doi.org/10.1016/j.jmatprotec.2015.01.025

128. Junfeng L, Zhengying W (2017) Process optimization and microstructure characterization of ti6al4v manufactured by selective laser melting. IOP Conf Ser Mater Sci Eng 269(1):012026. https://doi.org/10.1088/1757-899X/269/1/012026

129. Pal S, Lojen G, Kokol V, Drstvensek I (2018) Evolution of metallurgical properties of Ti-6Al-4V alloy fabricated in different energy densities in the selective laser melting technique. J Manuf Process 35:538–546. https://doi.org/10.1016/j.jmapro.2018.09.012

130. Tian Y, Tomus D, Rometsch P, Wu X (2017) Influences of processing parameters on surface roughness of Hastelloy X

produced by selective laser melting. Addit Manuf 13:103–112. https://doi.org/10.1016/j.addma.2016.10.010

131. Chen Z, Wei Z, Wei P, Chen S, Lu B, Du J, Li J, Zhang S (2017) Experimental research on selective laser melting AlSi10Mg alloys: process, densification and performance. J Mater Eng Perform 26(12):5897–5905. https://doi.org/10.1007/s11665-017-3044-5

132. Attar H, Prashanth KG, Chaubey AK, Calin M, Zhang LC, Scudino S, Eckert J (2015) Comparison of wear properties of commercially pure titanium prepared by selective laser melting and casting processes. Mater Lett 142:38–41. https://doi.org/10.1016/j.matlet.2014.11.156

133. Foudzi FM, Jamhari FI, Buhairi MA (2020) Effect of processing parameters on microhardness and microstructure of additive manufactured titanium alloy (Ti6Al4V) via selective laser melting (SLM). In: Proceedings of Mechanical Engineering Research Day, pp 55–57

134. ASTM International (2010) Standard specification for titanium-6aluminum-4vanadium alloy castings for surgical implants (UNS R56406). ASTM F1108-04. https://www.astm.org/standards/f1108. Accessed 10 Mar 2022

135. Tao P, Li HX, Huang BY, Hu QD, Gong SL, Xu QY (2018) Tensile behavior of Ti-6Al-4V alloy fabricated by selective laser melting: effects of microstructures and as-built surface quality. China Foundry 15(4):243–252. https://doi.org/10.1007/s41230-018-8064-8

136. Ur Rehman A, Mahmood MA, Ansari P, Pitir F, Salamci MU, Popescu AC, Mihailescu IN (2021) Spatter formation and splashing induced defects in laser-based powder bed fusion of AlSi10Mg alloy: a novel hydrodynamics modelling with empirical testing. Metals 11(12):2023. https://doi.org/10.3390/met11122023